RESEARCH PAPER

Effects of supporting plate hole and welding force on weld formation and mechanical property of friction plug joints for AA2219-T87 friction stir welds

Bo Du[1] · Xinqi Yang[1] · Kaixuan Liu[1] · Zhuanping Sun[1,2] · Dongpo Wang[1]

Abstract
Friction plug welding (FPW) experiments were performed on 8-mm-thick 2219-T87 FSW welds to investigate the weld formation, microstructure, hardness distribution, mechanical property, and fracture behaviors of FPW joint. The main findings are as follows: geometric size of supporting plate hole and welding force exert great effect on weld formation and mechanical property. Recrystallized zone (RZ) with varied width is observed on the bonding interface between the plug and base metal due to huge friction heat and deformation. Softening is found near the bonding interface due to the disappearance of cold working and transformation of constituent particles. The ultimate tensile strength (UTS) and elongation of FPW joint can reach 336.3MPa and 8%, respectively. The initial fracture of tensile specimen is prone to locate at the lower part of RZ. The tensile fracture morphology of FPW joint is characterized by dimples.

Keywords Friction plug welding · AA2219-T87 aluminum alloy · FSW weld · Supporting plate hole · Microstructure · Mechanical property

1 Introduction

The aluminum alloy 2219-T87 has become the preferred structural material in liquid rocket propellant storage tank structure due to its low density, high strength, and admirable cryogenic property compared with other aluminum alloys [1, 2]. Friction stir welding (FSW) and bobbin tool friction stir welding (BTFSW) have been widely applied in manufacturing longitudinal and circumferential welds of storage tank for its great advantages such as energy efficient, environment friendly, and versatile [3, 4]. However, a keyhole defect (it is a through hole for BTFSW) will be left at the termination of weld, which should be perfectly repaired.

Friction plug welding (FPW) is a solid-state welding technique exhibiting dominant advantages such as high joint strength, low residual stress, and very small distortion over tungsten inert gas welding (TIG) methods and has become the most promising technique in repairing terminal keyhole or through hole, as well as other defects formed in a TIG or FSW weld. As Hartley revealed, the ultimate tensile strength (UTS) of FPW joint increased by 20% compared with traditional TIG repair method [5].

Since the invention of FPW technique, Lockheed Martin, Marshall Flight Center and TWI initiate the investigation on FPW owing to its dominant advantages. To obtain high-strength FPW welds, the design of plug and plate hole was optimized [6, 7]. In addition, the "top hat" and "heat sink" were designed on the plug to increase the friction heat and pressure and eliminate weak-bonding defects [8, 9]. Metz and Barkey investigated the microstructure and fatigue behavior of 2195 Al-Li FPW joints that contain FSW welds. In their study, a 30–122-μm recrystallized layer and a 35% reduction of hardness were observed at the weld interface. The fatigue behavior decreased compared with FSW joint, which was determined by a complex effect of base metal, friction stir weld,

---

Recommended for publication by Commission III - Resistance Welding, Solid State Welding, and Allied Joining Process

✉ Xinqi Yang
   xqyang@tju.edu.cn

1   Tianjin Key Laboratory of Advanced Joining Technology, School of Materials Science and Engineering, Tianjin University, Tianjin 300350, People's Republic of China

2   Tianjin Long March Rocket Manufacture Co., Ltd., Tianjin 300451, People's Republic of China

Fig. 1 The schematic illustration of FPW repairing process: **a** welding process and **b** surface smoothing process
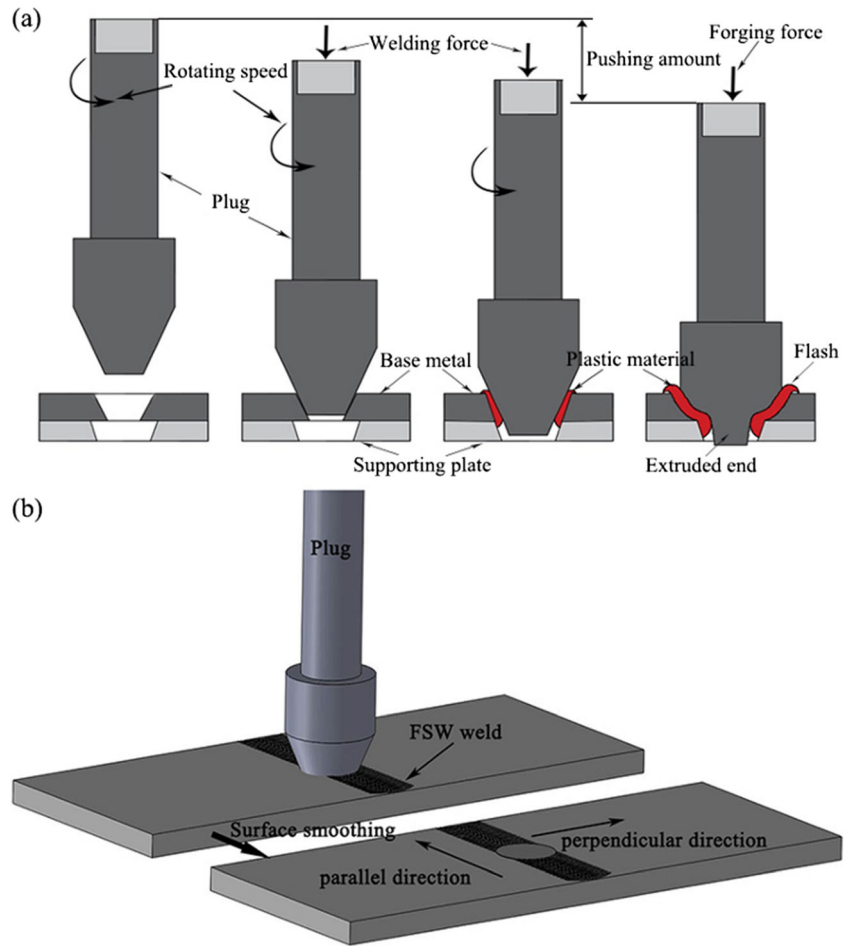

Fig. 2 Geometric dimensions of **a** plug and plate hole, **b** supporting plate hole, and **c** tensile specimen
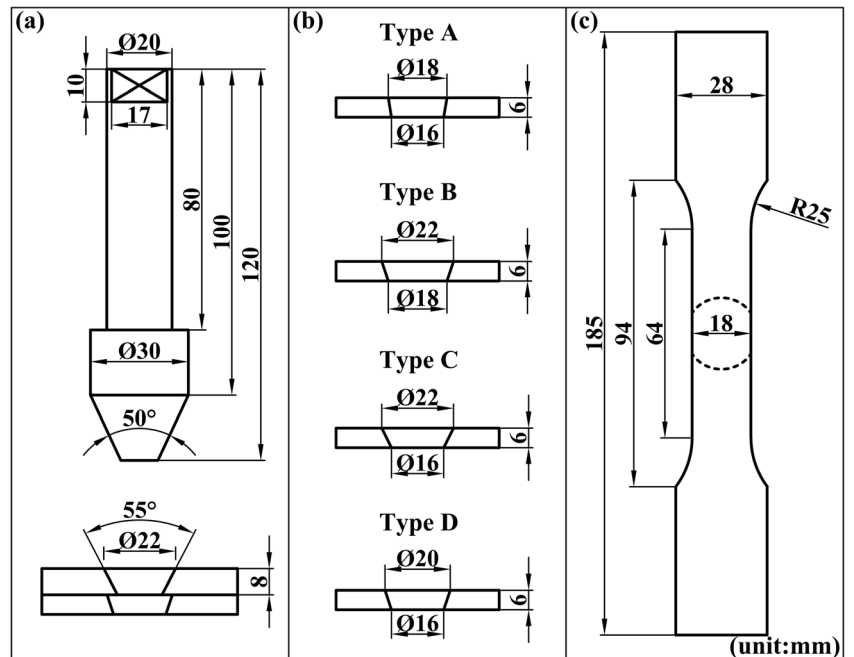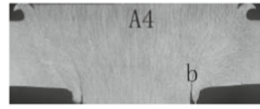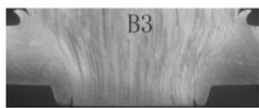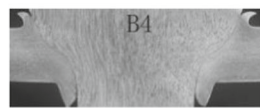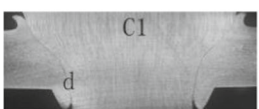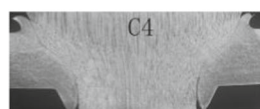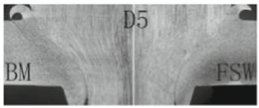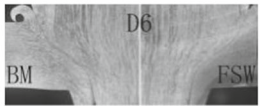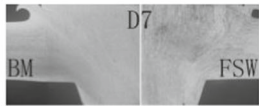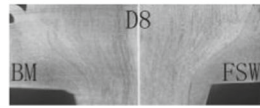
Table 1 Welding parameters and specimen no.
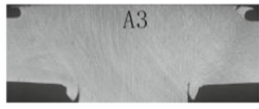
Specimen no.	Supporting plate hole	Rotational speed (kN)	Welding force (kN)	Forging force (kN)	Pushing amount (mm)
A1	Type A	7500	20	25	6
A2		7500	25	30	6
A3		7500	30	35	6
A4		7500	35	40	6
B1	Type B	7500	20	25	6
B2		7500	25	30	6
B3		7500	30	35	6
B4		7500	35	40	6
C1	Type C	7500	20	25	6
C2		7500	25	30	6
C3		7500	30	35	6
C4		7500	35	40	6
D1	Type D	7500	20	25	6
D2		7500	25	30	6
D3		7500	30	35	6
D4		7500	35	40	6
D5		7500	40	45	6
D6		7500	45	50	6
D7		7500	50	55	6
D8		7500	55	60	6

Supporting plate hole	Welding force (kN)			
	20kN	25kN	30kN	35kN
Type A *	A1 2mm	A2 a	A3	A4 b
Type B *	B1 c	B2	B3	B4
Type C *	C1 d	C2 e	C3	C4
Type D *	D1	D2	D3	D4 f
	40kN	45kN	50kN	55kN
Type D **	D5 BM FSW	D6 BM FSW	D7 BM FSW	D8 BM FSW

* Cross-section appearance along the parallel direction of FSW weld; ** One half cross-section appearance along the parallel direction of FSW weld, the other half along the perpendicular direction

Fig. 3 Macroappearances of FPW joints

Table 2 Estimated results of weld quality

Welding force (kN)	Supporting plate hole			
	Type A	Type B	Type C	Type D
20	▲	◆	◆	◆
25	▲	◆	◆	●
30	▲	◆	●	●
35	▲	●	●	●
40	–	–	–	●
45	–	–	–	●
50	–	–	–	●
55	–	–	–	●

▲ Macrodefect, ◆ weak-bonding, ● defect-free

and FPW joint [10–12]. Du et al. clarified the characteristics of weld formation, microstructure, and mechanical property, as well as the relationship between local microstructural evolution and tensile behavior of FPW joint for AA2219-T87 [13, 14]. Hynes et al. reported the bonding features of FPW joint between Ti-6Al-4V and AA2024 aluminum alloy; the Charpy impact of the joint could reach 284.36 kJ/m^2 [15]. Furthermore, Hynes et al. proposed an analytical modeling, which revealed the effect of friction time and preheating on temperature distribution [16, 17]. Zuo et al. also proposed an analytical mechanic model of FPW process, while his model neglected the deformation of plug [18].

The repairing quality of FPW technique directly determines the global reliability of storage tanks. So far, there are few public results on FPW for FSW weld. In FPW process, there are many factors that involved in the repair quality, including welding parameters, dimensions of plug and plate hole, as well as dimensions of supporting plate hole. Among these influencing factors, the welding force and dimension of supporting plate hole are of great significance. The influences of supporting plate hole and welding force on weld formation and mechanical property of FPW joint have not been clearly clarified, which deserve a detailed investigation.

The present paper revealed the influence of supporting plate hole on weld formation and mechanical property of FPW joint for FSW weld. Furthermore, characteristics of weld formation, microstructure, hardness distribution, and failure mechanism of FPW joint were clarified. The present research will provide some theoretical support for the engineering application of FPW technique in repairing FSW defects.

2 Experimental procedures

In the present study, 8-mm-thick AA2219-T87 plates that contain FSW welds and AA2219-T87 plugs were selected to perform the FPW experiments. The dimensions of the plates are 200 mm × 80 mm × 8 mm. The measured UTS and elongation of FSW weld are about 325 MPa and 7%, respectively. The schematic illustration of FPW process is shown in Fig. 1.

All the FPW experiments were completed on the FPW system developed autonomously by Tianjin University. The geometric details of plug, plate hole, supporting plate hole, and tensile specimen are shown in Fig. 2. The welding parameters and specimen no. are listed in Table 1.

The as-welded specimens were cut along the parallel and perpendicular directions for macro- and micro-observation, as well as hardness test. The samples were ground with abrasive papers, mechanically polished with diamond metallographic polishing liquid, and then etched with Keller reagent (2 ml HF, 3 ml HCl, 5 ml HNO$_3$, 190 ml H$_2$O) for about 10 s. Macro- and micro-observations were performed on OLYMPUS GX51 optical microscope. With the OM observations finished, the Vickers hardness test was carried out using 432SVD Vickers microhardness tester. A 1000 g force and a dwell time of 10 s were adopted. The tensile tests were conducted according to standard procedure using the CSS-44100 universal testing machine with a cross-head traveling speed of 3 mm/min. The fracture morphologies of the failure specimens were examined in detail by Hitachi-S4800 scanning electron microscope.

3 Results and discussion

3.1 Macroappearances

All the cross-sectional appearances of FPW joints are shown in Fig. 3. As shown in Fig. 3, there are two types of flashes for each joint, which are the upper flash and the lower flash. In fact, both the two flashes are extruded plastic metal, which are associated with the weld formation of FPW joint. It can be seen from Fig. 3 that the areas of lower flash for FPW joints obtained at type A supporting plate are less than the others. Under a certain supporting plate, the area of lower flash increases with the increasing welding force.

Supporting plate hole	Welding force (kN)			
20 kN	25 kN		30 kN	35 kN
Type A*				
Type B*				
Type C*				
Type D*				
	40 kN		45 kN	50 kN	55 kN
Type D**				

*Cross-sectional appearance along the parallel direction of FSW weld

**One-half cross-sectional appearance along the parallel direction of FSW weld, the other half along the perpendicular direction

Each joint was examined through optical microscope detailed, and the estimated results of weld quality are shown in
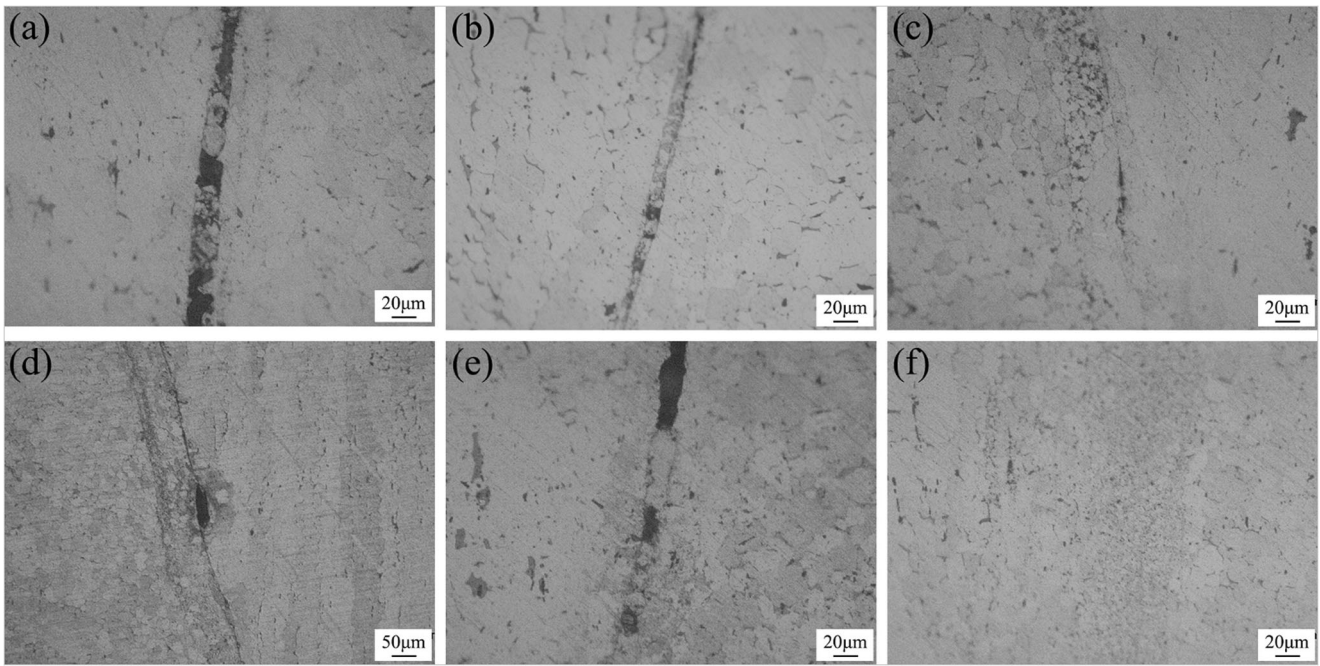
Fig. 4 Magnified images of regions marked in Fig. 3: **a** region a, **b** region b, **c** region c, **d** region d, **e** region e, and **f** region f
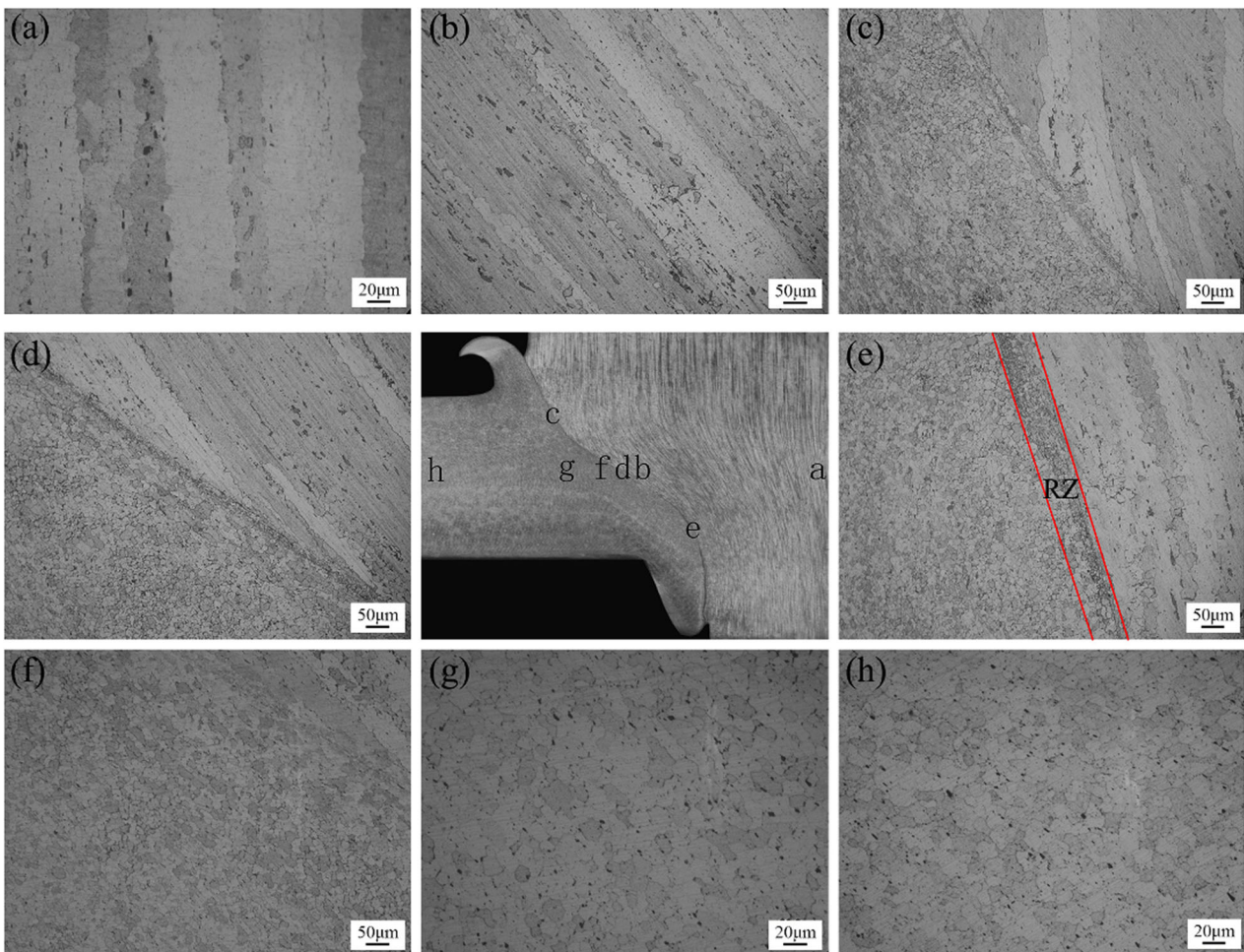

Fig. 5 Microstructures of D7 joint along the parallel direction of FSW weld: **a** PM, **b** PTMAZ, **c** upper RZ, **d** middle RZ, **e** lower RZ, **f** TMAZ, **g** HAZ, and **h** NZ
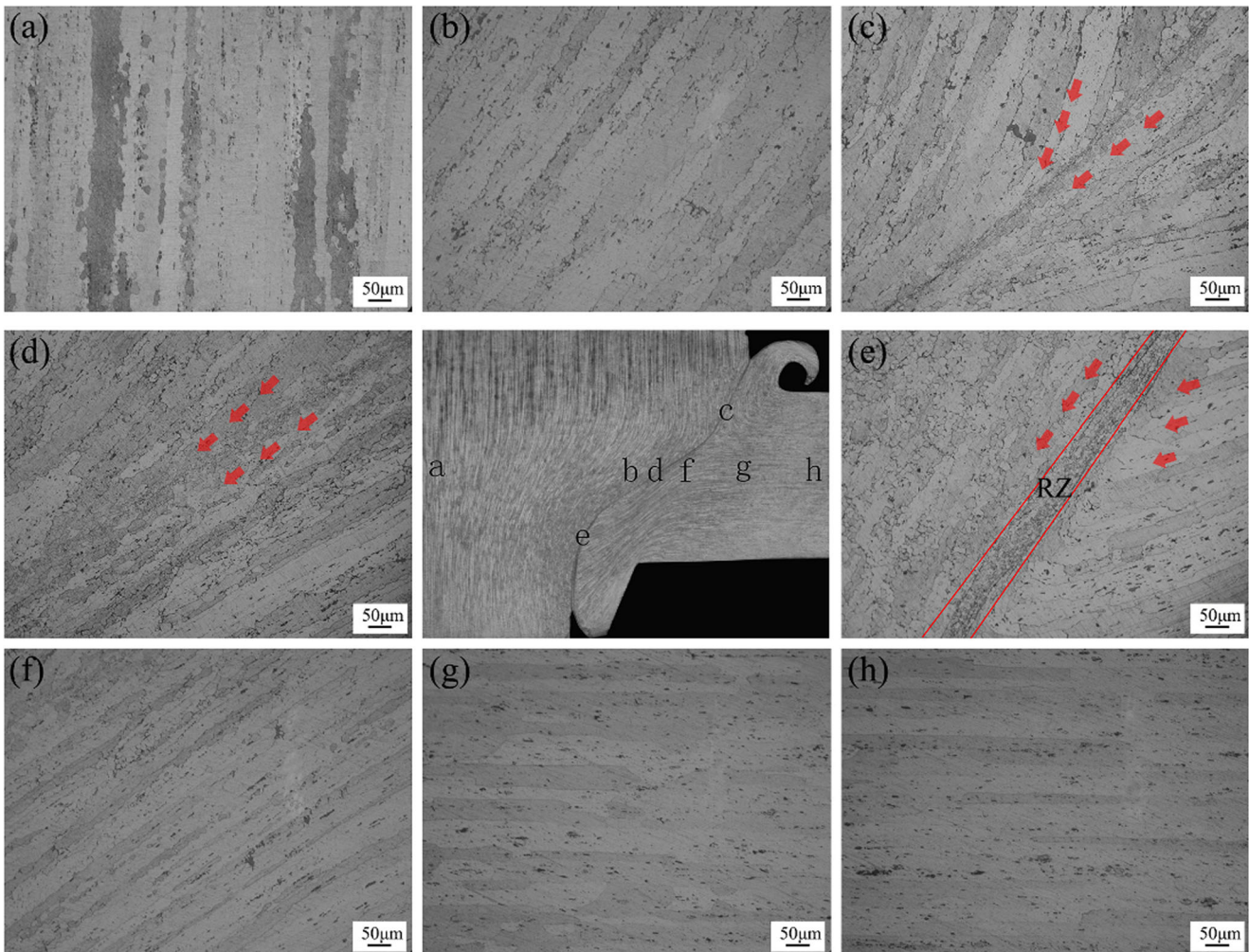
Fig. 6 Microstructures of D7 joint along the perpendicular direction of FSW weld: **a** PM, **b** PTMAZ, **c** upper RZ, **d** middle RZ, **e** lower RZ, **f** TMAZ, **g** HAZ, and **h** BM

Table 2. Figure 4 shows the magnified images of regions marked in Fig. 3. According to the estimated results, all the FPW joints are divided into three types, which are macrodefect joint, weak-bonding joint, and defect-free joint. The results indicate that the supporting plate hole and welding force exert significant effect on weld formation. For FPW process, macrodefect and weak-bonding defect are prone to form at the lower part of FPW joint owing to the poor friction heat and pressure. When using type A supporting plate, macrodefects exist at all the listed welding forces, and the defects are larger than the others (as shown in Fig. 4a, b). When using type B and type C supporting plate, weak-bonding defects are observed at a welding force of 20 kN and 25 kN, the defects become small and discontinuous compared with that of type A (as shown in Fig. 4c–e). As the welding force increases to 30 kN and 35 kN, no observable defects are found. When using type D supporting plate, defect-free joints are obtained when the welding force is higher than 25 kN (as shown in Fig. 4f). Based on the above

results, it could be seen that the weld formation indicates obvious improvement with the increasing welding force. Besides, it also could be concluded that type D supporting plate exhibits wider process window for obtaining defect-free joints than the others. Therefore, more FPW experiments were conducted based on type D supporting plate.

In FPW process, the supporting plate hole has two main functions; one is to receive the extruded plastic materials, and the other one is to provide supporting to ensure effective friction between the plug and base metal. In the case of type A supporting plate, the hole is too small to hold enough flashes at the bottom, and material flow is constraint. The defects cannot be extruded into the hole and left in the base metal. When the supporting plate hole gets larger (type B and type C supporting plate), the hole is capable to hold enough extruded materials, while the sidewall of hole cannot provide enough supporting force to ensure the effective friction between plug and base metal. As a result, weak-bonding defect formed in this case. For a certain supporting plate, the increasing
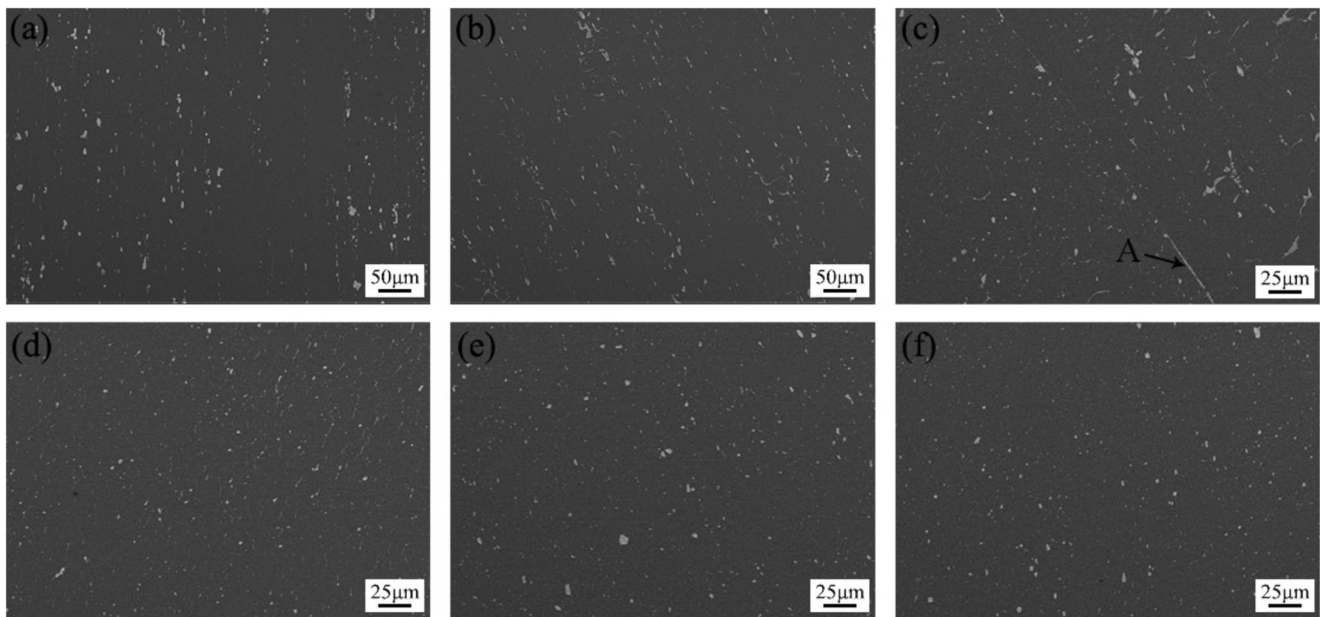
Fig. 7 SEM observations of FPW joint using 45 kN welding force along the parallel direction of FSW weld: **a** PM, **b** PTMAZ, **c** RZ, **d** TMAZ, **e** HAZ, and **f** NZ

welding force will extrude the defects into the supporting plate hole and meantime ensure enough friction force between plug and base metal; thus, the weld quality could be improved.

3.2 Microstructures

Figures 5 and 6 illustrate the cross-sectional microstructures of FPW joint along the parallel and perpendicular direction of FSW weld, respectively. The whole joint can be divided into

six regions: plug metal (PM), plug thermomechanically affected zone (PTMAZ), recrystallized zone (RZ), thermomechanically affected zone (TMAZ), heat-affected zone (HAZ), and nugget zone (NZ)/base metal (BM). In these two directions, recrystallization is observed on the bonding interface, which is related to the actions of drastic friction heat and material flow. The width of RZ is changing from the upper part to the lower part (as shown in Figs. 5c–e and 6c–e). It is about 10–15 μm in upper and middle part of bonding
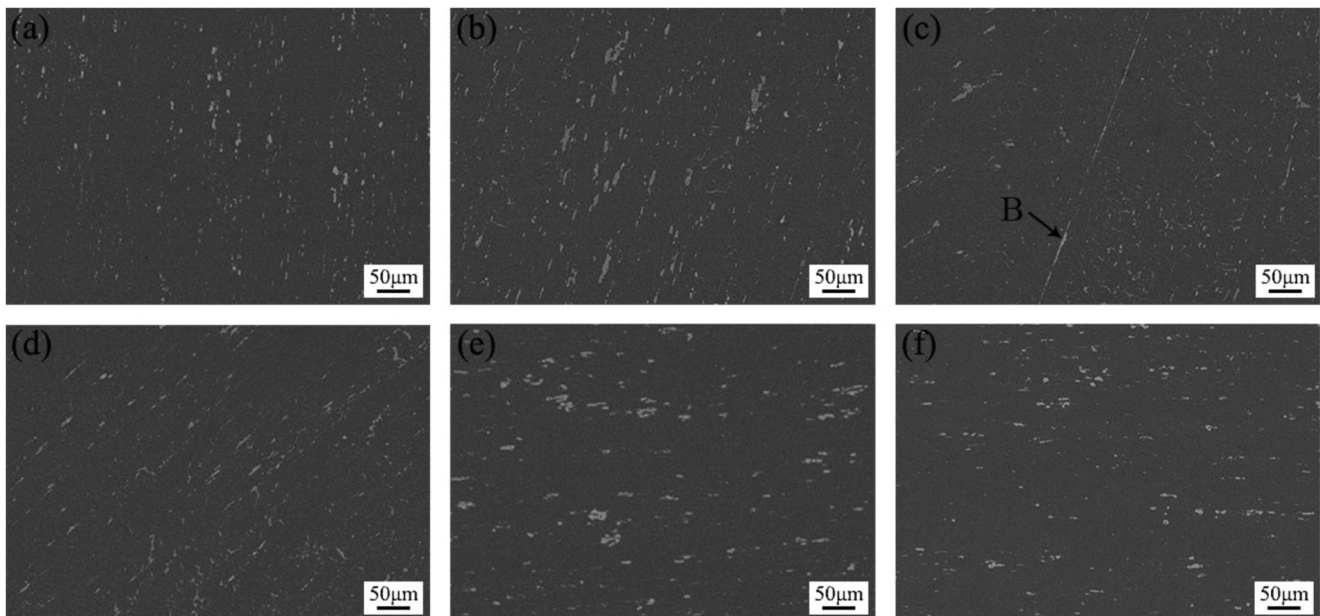

Fig. 8 SEM observations of FPW joint using 45 kN welding force along the perpendicular direction of FSW weld: **a** PM, **b** PTMAZ, **c** RZ, **d** TMAZ, **e** HAZ, and **f** BM
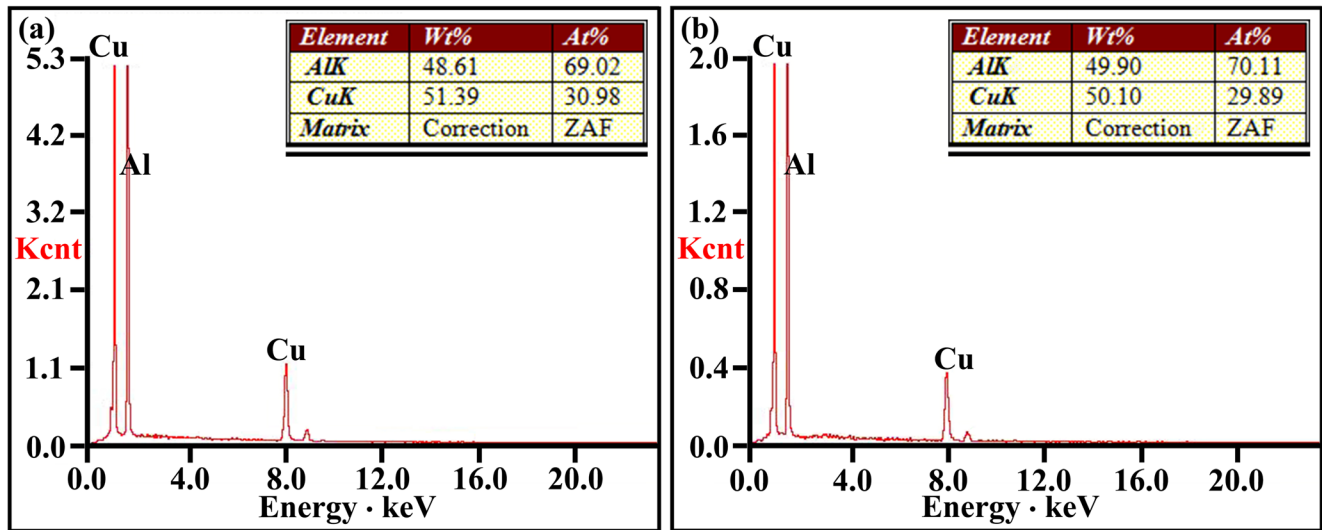
Fig. 9 EDS results of **a** particle A and **b** particle B on the bonding interface marked in Figs. 7 and 8

interface, while reaches 60 μm at the lower part of RZ. The varied width of RZ is related to the different material flow and friction time.

In PM, the grains only affected by the friction heat and remained the initial grain structure (as shown in Figs. 5a and 6a). In PTMAZ relatively away from the bonding interface, the grains are severely deformed compared with that of PM due to the double effect of heat and force (as shown in Figs. 5b and 6b). In PTMAZ close to the bonding interface, the grains are partially recrystallized. This partially recrystallized trend gets more obvious from upper part to lower part owing to the increased friction time (as shown in Figs. 5c–e and 6c–e). In TMAZ of parallel direction, the equiaxed grains are elongated with no partially recrystallization observed (as shown in Fig. 5f). In TMAZ of perpendicular direction, the grains are also elongated with no obvious partially recrystallization observed. The grains present varied orientations and get slim from upper part to lower part, indicating larger plastic deformation in lower TMAZ (as shown in Fig. 6c–e). In HAZ, the grains only influenced by the friction heat and the grain size indicates a small increase in parallel direction, while the increase of grain size is negligible in perpendicular direction. For BM and NZ, the grains are free of the effect of friction heat and welding force, which remain the initial grain structure.

Besides the grain structure, the constituent particles also suffered significant change owing to the friction heat and axial force. In FPW process, dissolution of θ′ phases, coarsening of θ phases, and the transformation of θ′ phases to θ phases all happened owing to the thermal cycle. The T87 state indicates that AA2219 aluminum alloy is strengthened by solution treated and then hardened by cold work. So the change of constituent particles will greatly affect the mechanical property of FPW joint.

Figures 7 and 8 show the distributions of constituent particles on cross-sectional surface of D7 joint along the parallel/perpendicular direction. The constituent particles in PM exist in grains and grain boundaries along the drawing direction (as shown in Figs. 7a and 8a). Compared with PM, the constituent particles in PTMAZ suffered significant deformation and shape change (as shown in Figs. 7b and 8b). In RZ, the constituent particles get refined, but linear constituent particles are found at local position (as shown in Figs. 7c and 8c). The energy dispersion spectrum (EDS) results of marked particles on the bonding interface are shown in Fig. 9. The main

Fig. 10 Hardness profiles of D7 joint: **a** parallel direction and **b** perpendicular direction
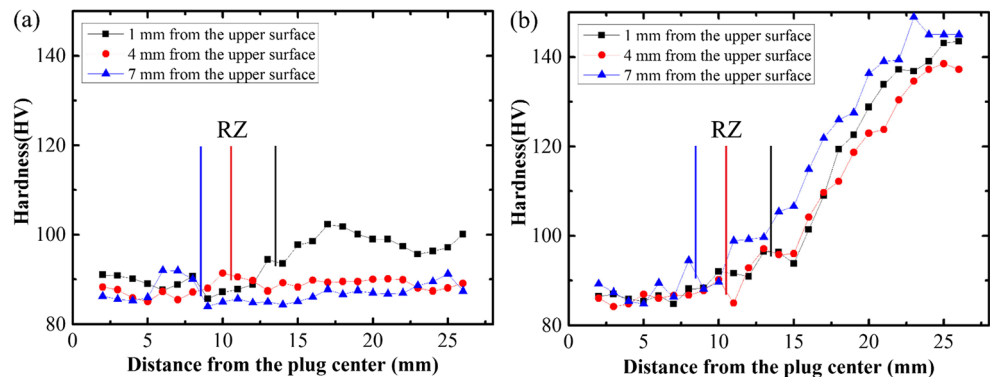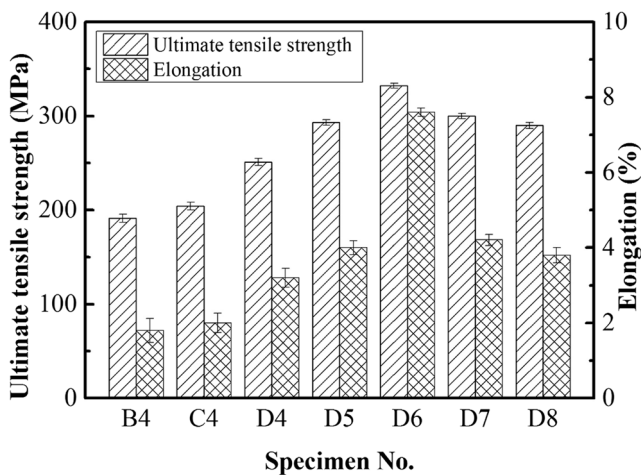
Fig. 11 Tensile properties of FPW joints

elements of the linear particles are Al and Cu, which is thought to be θ phases. In TMAZ, constituent particles in both parallel direction and perpendicular direction are elongated and showing obvious preferred orientation (as shown in Fig. 7d and 8d). In HAZ, constituent particles coarsened and big-size particles increase significantly (as shown in Figs. 7e and 8e).

3.3 Hardness profiles

In order to analyze the hardness distribution of FPW joint, hardness tests were performed along the parallel and perpendicular directions. Three lines were measured and identified as upper, middle, and lower, which are 1 mm, 4 mm, and 7 mm from the upper surface. The hardness results and the positions of RZ at each line are presented in Fig. 10.

As shown in Fig. 10, the hardness of plug zone decreases significantly compared with the initial hardness of plug (141 HV), ranging from 85 to 90 HV. The cooling condition of plug is poorer than base metal, and the whole plug is affected by thermal cycle. Generally speaking, the hardness of RZ indicates a descending trend from upper part to lower part,
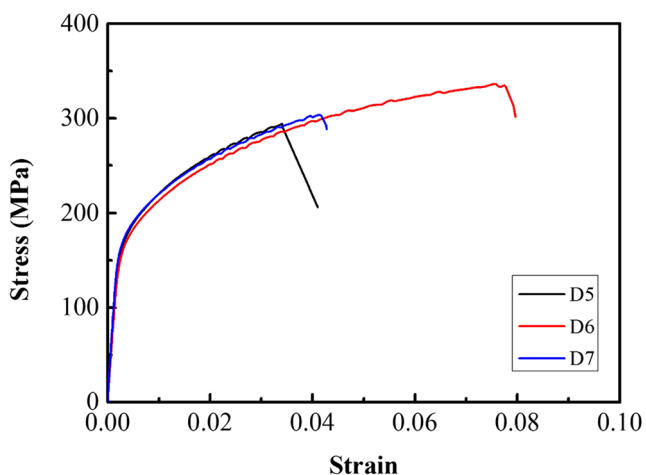

Fig. 12 Stress-strain curves of FPW joints

which is related to the increasing grain size caused by the increasing friction time. In addition, the hardness of RZ is also a little higher than the adjacent TMAZ and PTMAZ, which is resulted from the smaller grain size in RZ than TMAZ and PTMAZ. In parallel direction, the hardness indicates small increase from TMAZ to the NZ. The hardness in the NZ shows a descending trend from the upper part to lower part, which is related to the larger plastic deformation of upper part in FSW process. In perpendicular direction, the hardness also gradually increases from TMAZ to the BM. The hardness profile in perpendicular direction is similar to that of FPW joint of base metal.

3.4 Tensile properties

Tensile tests are performed in order to investigate the effects of supporting plate hole and welding force on the tensile property of FPW joints. For each welding condition, three specimens were tested, and the results are shown in Fig. 11. The stress-stain curves of selected joints are shown in Fig. 12.

As shown in Fig. 11, it is clearly seen that the geometric size of supporting plate hole has great effect on the UTS and elongation of FPW joints at the same welding condition. Combined with the results in Fig. 3 and Table 2, it is concluded that type D supporting plate is prone to form high-quality FPW joint. Except for supporting plate hole, welding force also exhibits important effect on the mechanical property of FPW joints. The UTS and elongation continue increasing as the welding force ranges from 35 to 45 kN. The average UTS is only 251 ± 3.8 MPa at a welding force of 35 kN (D4 joint), and the highest UTS (336.3 MPa) and elongation (8%) are obtained at a welding force of 45 kN. The UTS and elongation of optimized FPW joint are equivalent to that of FSW joint, which are approximately 73.9% and 66.7% of base metal.

3.5 Fracture features

Figure 13 presents the typical fracture positions of FPW joints. It is seen that the fracture path involves PTMAZ, RZ, and TMAZ. FPW joint indicates huge microstructure inhomogeneity from upper part to lower part, which will certainly influence the fracture behavior of the joint. Thus, the fracture path is determined by a complex influence of defects, softening in TMAZ and PTMAZ, and huge microstructure inhomogeneity near bonding interface. The lower part of RZ is the weakest zone owing to the inadequate friction heat and force. Thus, the initial fracture locates at the lower part of RZ and then propagates along the weak area of PTMAZ, RZ, and TMAZ.

Figure 14a, e is macroappearances of fractured tensile specimen. Figure 14b–d illustrates the detailed fracture surfaces of regions A, B, and C. Figures 14f–h illustrates the detailed fracture surfaces of at regions D, E, and F. It can be seen that the fracture of upper part and middle part locates at the

Fig. 13 Fracture positions of **a** D4 joint and **b** D6 joint
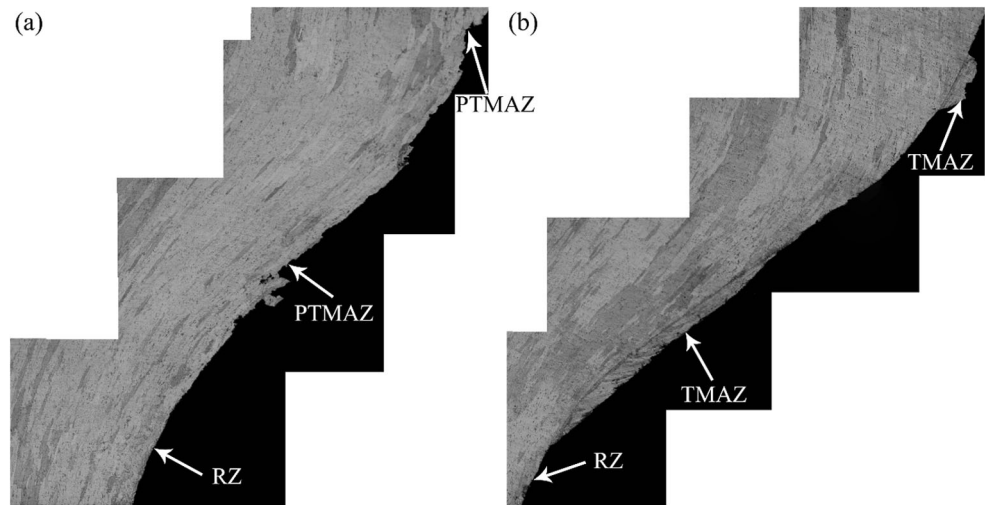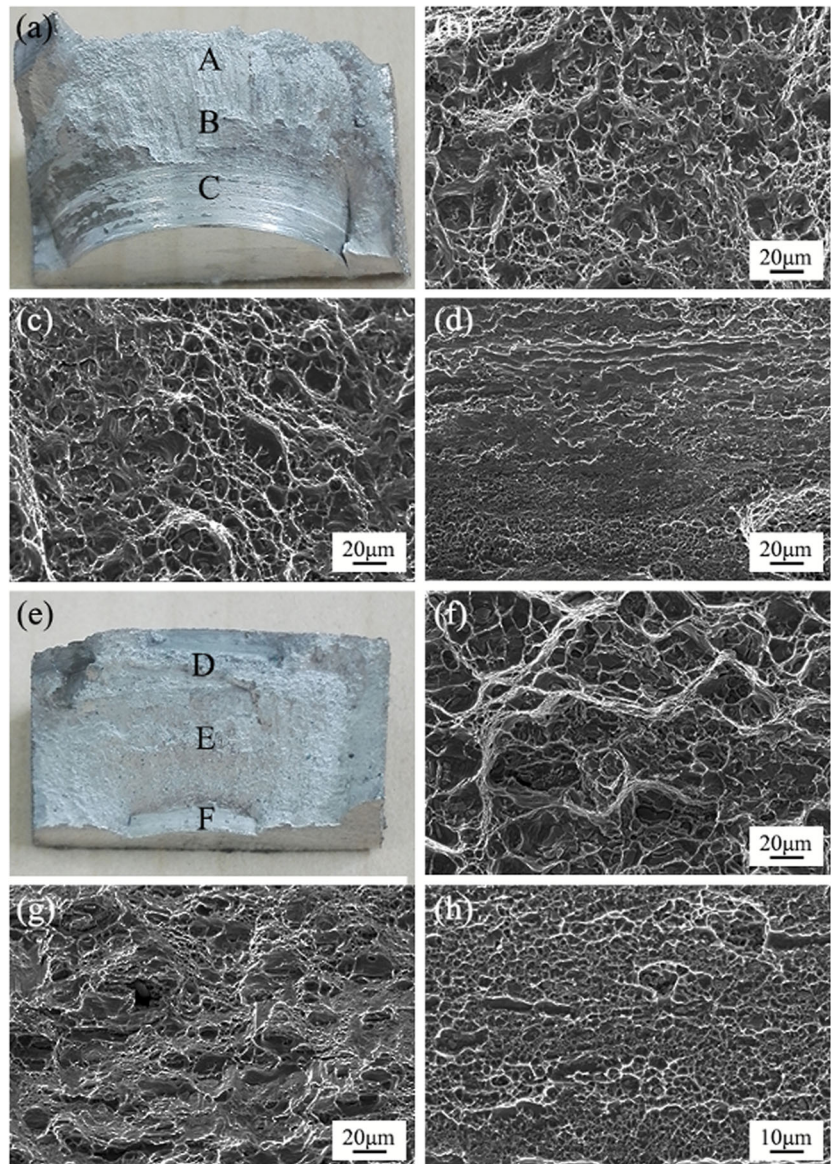

Fig. 14 Fracture morphologies of **a** macroappearance, **b** region A, **c** region B, **d** region C marked in **a** for D4 joint and **e** macroappearance, **f** region D, **g** region E, and **h** region F marked in **e** for D6 joint
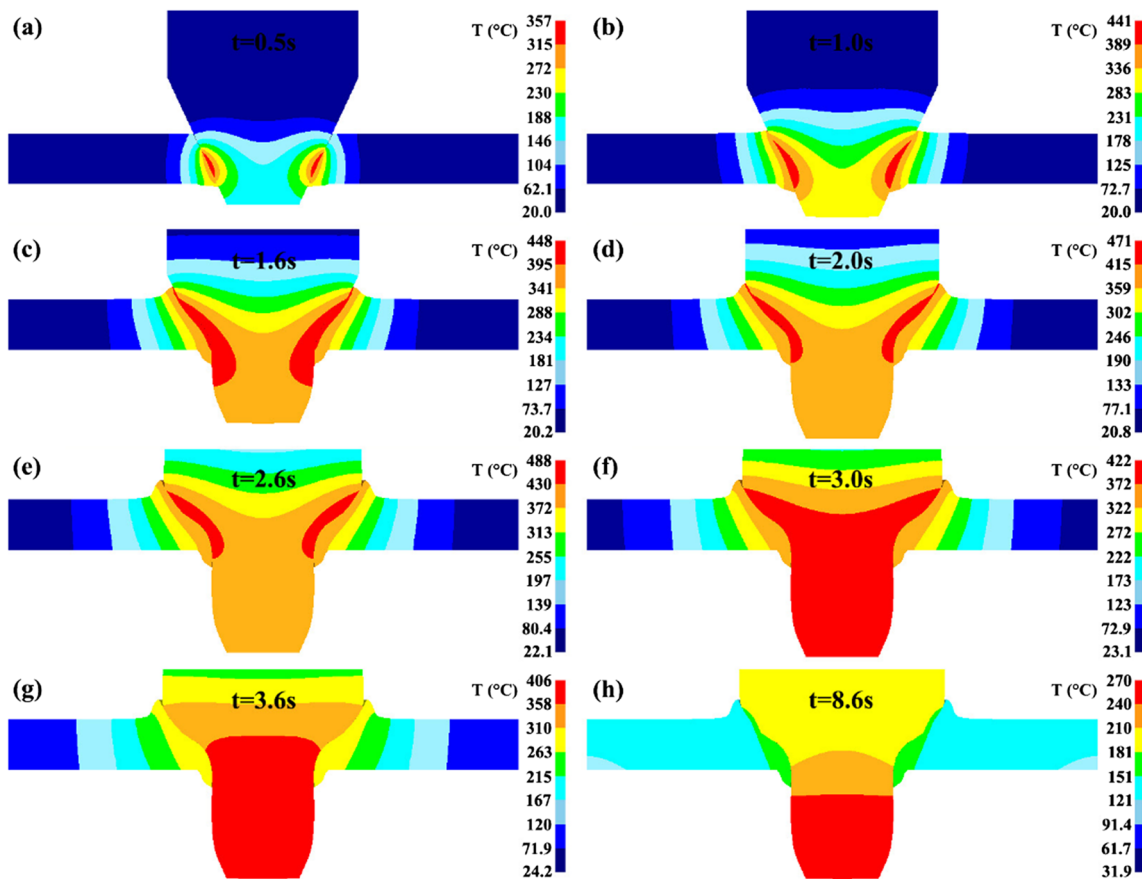
Fig. 15 Temperature contour on the cross section of D7 joint

PTMAZ or TMAZ. The fracture surfaces of these positions are characterized by larger and deep dimples, implying large plastic deformation (as shown in Fig. 14b, c, f, g). But at the lower part, the fracture surfaces of D4 are almost plain with few dimples, indicating the poor connection (as shown in Fig. 14d). For D6 joint, small and shallow dimples distribute at the

lower part while with no appearance of original surfaces of plug and hole (as shown in Fig. 14h). According to the fracture morphology of FPW joint, it is concluded that the lower part of RZ is the weakest zone across the whole joint. To obtain high-quality FPW joints, improving the connection quality of the lower part bonding interface is of great significance.
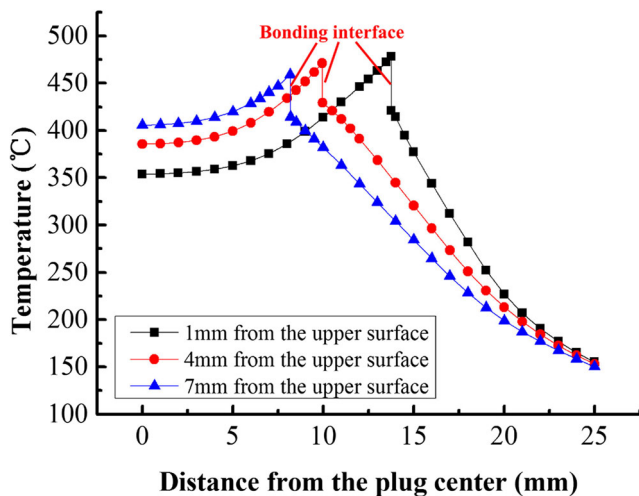
3.6 Temperature distributions

To identify the thermal characteristics of FPW process, a Lagrangian, thermomechanical coupled finite element model with a rigid-viscoplastic (RVP) material behavior is developed based on Deform software. For FPW process of FSW weld, a taper through hole is drilled. According to the macrostructure and microstructure shown in Fig. 6, most part of the initial FSW weld is removed in perpendicular direction, whose effect on FPW process could be neglected. Thus, the plate to be welded is assumed to be uniform base metal.

Figure 15 exhibits the temperature distributions on the cross section of D7 joint during FPW process. According to Fig. 15, the lower part of the joint is frictional heated

Fig. 16 Temperature profiles of D7 joint at different thickness at 2.6 s

firstly owing to the angle difference between the plug and base metal. Then, the contact area continues increasing and moving upwards (as shown in Fig. 15a, b). With full contact achieved, the deformation of bonding interface is observed and intensifies with the conduction of welding process (as shown in Fig. 15c–f). In this stage, the increase rate of temperature gradually slows down, while high-temperature zone continues spreading. As shown in Fig. 15g, the temperature begins to decrease due to the stalling of weld machine. In forging stage finished, a forging force is exerted and lasts for 5 s; the whole joint gradually cools down (as shown in Fig. 15h).

Figure 16 shows the temperature profiles of D7 joint at different thickness at 2.6 s. According to Fig. 16, the bonding interface indicates higher temperature compared with PM and BM. There is a temperature difference on two sides of the bonding interface. The temperature at plug side is about 50 °C higher than that of the base metal side, which is caused by the different heat dissipation condition. Combining the hardness profile and temperature profile at the position of 4 mm from the upper surface, it could be concluded that the terminal line of HAZ is at the position of 22.5mm from the plug center for D7 joint. That is, the temperature inside HAZ is higher than 180 °C for D7 joint. Outside this terminal line, the position is free of thermal effect.

4 Conclusions

Based on the above results, main conclusions can be derived as follows:

1. FPW experiments are performed on 8-mm-thick FSW weld, and defect-free joints are obtained. The geometric size of supporting plate hole and welding force exert great effect on the weld formation. Type D supporting plate and higher welding force are prone to obtain defect-free FPW joints.
2. RZ is formed on the bonding interface between the plug and base metal, and the width of the RZ is inhomogeneous along the thickness of the joint. The lower part indicates larger width of RZ owing to the material flow and long friction time.
3. Local softening is found in PM, PTMAZ, RZ, TMAZ, and HAZ owing to the friction heat. The UTS and elongation of FPW joint can reach 336.3 MPa and 8%, approximately 73.9% and 66.7% equivalent to that of the base metal.
4. The initial fracture of FPW joints locates at the lower part of RZ and then propagates among PTMAZ, RZ, and TMAZ. The upper part and middle part of fractured tensile specimen indicate larger and deeper dimples than the lower part.

References

1. Jha AK, Ramesh Narayanan P, Sreekumar K (2009) Liquation cracking of Al-6.3 Cu alloy propellant storage tank—a case study. Eng Fail Anal 16(5):1587–1596
2. Malarvizhi S, Raghukandan K, Viswanathan N (2008) Fatigue behaviour of post weld heat treated electron beam welded AA2219 aluminium alloy joints. Mater Des 29(8):1562–1567
3. Arora KS, Pandey S, Schaper M, Kumar R (2010) Effect of process parameters on friction stir welding of aluminum alloy 2219-T87. Int J Adv Manuf Technol 50(9–12):941–952
4. Horton KR (2011) Microhardness, strength and strain field characterization of self-reacting friction stir and plug welds of dissimilar aluminum alloys. Dissertation, University of Alabama
5. Hartley PJ (2000) Friction plug weld repair for the space shuttle external tank. NASA Document. Document ID 20000093962
6. Coletta ER, Cantrell MA (2001) Friction pull plug welding: dual chamfered plate hole. United States Patent. Patent No. 6230958B1
7. Takeshita R, Hibbard TL (2001) Friction pull plug welding. United States Patent. Patent No. 6213379B1
8. Coletta ER, Cantrell MA (2002) Friction pull plug welding: top hat plug design. United States Patent. Patent No. 6386419B2
9. Coletta ER, Cantrell MA (2005) Friction pull plug welding: chamfered heat sink pull plug design. United States Patent. Patent No. 6880743B1
10. Metz DF, Weishaupt ER, Barkey ME, Fairbee BS (2012) A microstructure and microhardness characterization of a friction plug weld in friction stir welded 2195 Al-Li. J Eng Mater Technol 134(2):021005
11. Metz DF, Barkey ME (2012) Fatigue behavior of friction plug welds in 2195 Al-Li alloy. Int J Fatigue 43:178–187
12. Metz DF, Barkey ME et al Experimental and numerical characterization of the fatigue and fracture properties of friction plug welds in 2195-T8 aluminum lithium alloy. Dissertation, University of Alabama
13. Du B, Sun Z, Yang X et al (2016) Characteristics of friction plug welding to 10mm thick AA2219-T87 sheet: weld formation, microstructure and mechanical property. Mater Sci Eng A 654:21–29
14. Du B, Cui L, Yang X et al (2017) Weakening mechanism and tensile fracture behavior of AA 2219-T87 friction plug welds. Mater Sci Eng A 693:129–135
15. Hynes NRJ, Velu PS, Nithin AM (2018) Friction push plug welding in airframe structures using Ti-6Al-4V plug. J Brazilian Soc Mech Sci Eng 40(3):158
16. Hynes NRJ, Nagaraj P, Thanga Kumar P (2014) Mathematical modeling of friction plug welding with preheating effect. Adv Mater Res 984-985:600–603
17. Hynes NRJ, Nithin AM (2016) Simulation on friction taper plug welding of AA6063-20Gr metal matrix composite. AIP Conference Proceedings 1728(1):020544
18. Zuo QK, Nunes AC Jr (2015) Mechanics model of plug welding. NASA Document Document ID 20150019530